AIR DAMPING ANALYSIS OF A DIFFERENTIAL CAPACITIVE ACCELEROMETER

Janderson Rocha Rodrigues, jrr@ita.br
Aeronautics Institute of Technology, 12228-900, São José dos Campos – SP – Brazil

André da Costa Teves, andreteves@gmail.com
School of Engineering, University of São Paulo, 05508-010, São Paulo – SP – Brazil

Angelo Passaro, angelo@ieav.cta.br
Institute for Advanced Studies, 12228-001, São José dos Campos – SP – Brazil

Luiz Carlos Sandoval Góes, goes@ita.br
Aeronautics Institute of Technology, 12228-900, São José dos Campos – SP – Brazil

Emilio Carlos Nelli Silva, ecnsilva@usp.br
School of Engineering, University of São Paulo, 05508-010, São Paulo – SP – Brazil

Carlos Fernando Rondina Mateus, mateus@ieav.cta.br
Institute for Advanced Studies, 12228-001, São José dos Campos – SP – Brazil

Abstract. *We describe the behavior of the gas between the electrodes of a capacitive accelerometer with the compressible-gas-film Reynolds equation, which relates pressure, density, viscosity and the surface velocity for the specific geometry of bounded film. This equation assumes that inertial forces are small compared to viscous forces, and that the gap is large compared to the mean free path of the gas. Assuming a small displacement of the moving electrode, small pressure variation around the ambient pressure and under the assumption of isothermal film, the analytical solution of the pressure is obtained. The pressure has two terms: one represents the damping and one represents the spring-like behavior of the gas. The integral of the pressure over the electrodes area lead directly to expressions for damping and air spring constant coefficients. The importance of compressible effects, represented by the spring constant coefficient, can be analized through of the squeeze number. For a very low squeeze number the incompressible–gas-film Reynolds equation can be utilized. When the pressure drops below the ambient pressure the modified Reynolds equation has to be used. For large displacement condition some models derived in the literature are presented. The validity of the analytical model is discussed according to the assumptions and simplifications made. Finally, all analytical results are compared with numerical results obtained by Computational Fluid Dynamics method (CFD) in both time-domain and frequency-domain. The results show very good agreement between the two methods, validating the analytical model for this kind of analysis.*

Keywords*: MEMS, accelerometer, differential capacitive, damping analysis, computational fluid dynamics method*

1. INTRODUCTION

The increasing demand for new applications has driven research and continuous development of traditional MEMS devices. This is the case, for instance, of micro-accelerometers and micro-gyroscopes for aerospace applications, as part of inertial measurement units (IMU's). For aerospace applications these devices must present high sensitivity while being immune to vibrations. If the sensors can be fabricated at low cost, several other markets would also absorb it, such as automotive sector.

In order to achieve these specifications, it is necessary to consider the interactions between the various physics domains involved in microsystems modeling. One of these interactions is between the moving mechanical components and the fluid surrounding them, what makes possible to find out the exact dynamic behavior of the structure. Once the main damping mechanism is known, it allows us to get the desired frequency response of the micro device by controlling the fluid pressure, viscosity coefficient or the gap layer, (Veijola *et. al.*, 1995).

In this work, we described the behavior of the gas in a differential capacitive accelerometer with the Reynolds equation. The validity of the analytical model is discussed according to the assumptions and simplifications made. Finally, all analytical results are compared with numerical results obtained by Computational Fluid Dynamics method (CFD) in both time-domain and frequency-domain.

2. ACCELEROMETER MODEL

The bulk-micromachined accelerometer simulated consists of a stack of three bonded silicon wafers, with the hinge springs and seismic mass incorporated in the middle one. The inertial mass forms a moveable inner electrode of a variable differential capacitor circuit, show in Fig 1. The two outer identical wafers are simply the fixed electrodes of the two capacitors. The differential capacitor senses the relative position of the inertial mass as it displaces under the

effect of an externally applied acceleration. Electronic circuit sense changes in capacitance, then convert them into an output voltage.

The geometric parameters of such device and properties of the gas are presented in Table 1. The data correspond to the values defined previously in the accelerometer design.

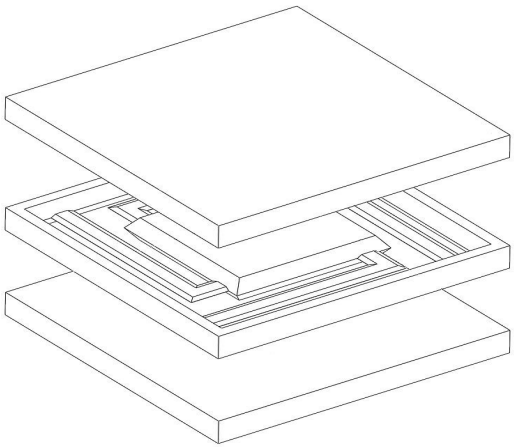

Figure 1. 3D views of the bulk-micromachined accelerometer.

Table 1. Some geometric parameters of the accelerometer and properties of the gas.

Description	Symbol	Value
Length of the seismic mass	L_m	$2x10^{-3}$ [m]
Width of the seismic mass	W_m	$2x10^{-3}$ [m]
Gap	h_o	$10x10^{-6}$ [m]
Natural frequency	ω_n	$16.022x10^{3}$ [rad/s]
Effective mass	M_{eff}	$4.2173x10^{-6}$ [kg]
Density of air(1)	ρ_o	1.184 [kg/m^3]
Ambient pressure	Pa	$101.325x10^{3}$ [Pa]
Mean free path of air	λ	$68.23x10^{-9}$ [m]
Viscosity of air(1)	η_o	18.192×10^{-6} [Pa.s]

(1) : measured at 25°C and ambient pressure .

In summary, the microfabrication of a bulk accelerometer involves a sequence of processes, e.g. thin film deposition, double face litography, simultaneous top and bottom wet etching, bonding of the three wafers.

The air trapped inside the set of wafers acts as a damping system when the seismic mass moves up and down due to an external acceleration acting in the normal direction to the seismic mass surface. In this work, we are mainly concerned with an analytical model to analyse the damping coefficient and its influence in the dynamic behavior of the silicon bulk-micromachined accelerometer, the electric forces are not taken into account.

3. ANALYTICAL APPROACH

Modeling of fluids can be divided into two big areas: molecular flow models and continuous flow models. The first one is subdivided in deterministic methods, e.g., Modern Molecular Dynamics Simulation (MD), and probabilistic methods as, e.g, Direct Simulation Monte Carlo (DSMC) and Boltzmann equations. In the second one, velocity, density, pressure, etc., are defined at every point in space and time, and conservation of mass, energy and momentum leads to a set of nonlinear partial differential equation as, e.g., Euler, Navier-Stokes and Burnett, (Gad-el-Hak, 2006).

Accelerometers total damping also can be divided into two main groups: the damping from the beams and the damping from the seismic mass. The main damping mechanisms associated to the beams vibrations are: internal material damping, thermoelastic damping, acoustic radiation effects in the interfaces and in the surrounding media, stick-slip at the clamped ends of the beams and the viscous damping, (Kaajakari, 2009).

Seismic mass damping is caused by viscous effects of the fluid on its top and bottom surfaces and by a parasitic couette flow between its lateral surface (mass thickness) and the inner middle wafer edges. Since in microscale the surface effects become more important than volumetric effects and the seismic mass top and bottom area is much bigger than the top and bottom beams area, the viscous damping due to seismic mass is the most important damping mechanism on the accelerometer structure. Likewise, the parasitic couette flow damping is negligible. However, when

the device operates in very low pressure, i. e., ultra-high vaccum, other damping sources as, for example, the internal material damping become a significant mechanism.

3.1. Squeeze Film Air Damping

The analysis of a Newtonian fluid in the laminar flow condition is done by the Navier-Stokes equations of motion. Two parallel plates, one movable (moving electrode) and one fixed (lower stationary electrode), with a thin layer of fluid between them are presented in Fig. 2. This problem is known as squeeze-film and has been resolved in lubrification theory through a derived form of Navier-Stokes equation, the Reynolds equation, (Gad-el-Hak, 2006).

The derivation of the Reynolds equation from the Navier-Stokes and Continuity equations is based on an analysis of an infinitesimal fluid element. The Reynolds equation also can be directly derived from Viscous Flow laws and principle of Mass Conservation. In both cases the high order terms of the inertia and viscous forces are neglected, (Bode, 2001).

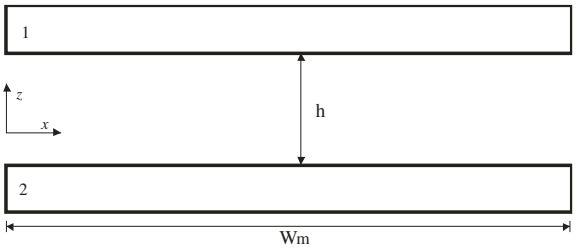

Figure 2. Two parallel plates separated by thin layer of a fluid.

The most general form of the bi-dimensional Reynolds equation is, (Gad-el-Hak, 2006):

$$\frac{\partial}{\partial x}\left(-\frac{\rho h^3}{12\eta}\frac{\partial p}{\partial x}\right)+\frac{\partial}{\partial z}\left(-\frac{\rho h^3}{12\eta}\frac{\partial p}{\partial z}\right)+\frac{\partial}{\partial x}\left[\frac{h\rho(u_1+u_2)}{2}\right]+\frac{\partial}{\partial z}\left[\frac{h\rho(v_1+v_2)}{2}\right]+ \\ +\rho(w_1-w_2)-\rho u_1\frac{\partial h}{\partial x}-\rho u_2\frac{\partial h}{\partial z}+h\frac{\partial \rho}{\partial t}=0 \tag{1}$$

where p is the pressure, $\rho(p)$ is the density and $\eta(p)$ is the viscosity coefficient of the fluid, $h(x,z,p)$ is the thickness of the fluid layer(gap of the capacitor), u_1 and u_2 are the velocities in the x-direction of top plate and the bottom plate, respectively, v_1 and v_2 are the velocities in the z-direction of the two plates, and w_1 and w_2 are the velocities of the fluid on the surfaces of the two plates.

The relation between the inertia forces and the viscous forces in squeeze-film problems is given by the modified Reynolds numbers R_s and R_L:

$$R_s=\frac{\omega\rho h^2}{2\pi\eta} \quad ; \quad R_L=\frac{V_x\rho h}{W_m\eta} \tag{2}$$

where V_x is the relative velocity in the x-direction, W_m is the plate width and ω is the plate movement frequency. The inertia effects can be ignored when both Reynolds numbers are smaller than unity. The device's supporting structure is several times more stiffer in the lateral direction than in the vertical one, thus, only vertical displacement of the plate is considered, i. e., $V_x = 0$ and therefore $R_L = 0$. The R_s number is dependent of the gap size and movement frequency , therefore the condition of $R_s < 1$ is only achieved when the gap is small or the movement frequency is not so high, (Veijola, 2004).

Neglecting the fluid inertial effects, Eq. (1) can be reduced to:

$$\frac{\partial}{\partial x}\left(\rho\frac{h^3}{\eta}\frac{\partial p}{\partial x}\right)+\frac{\partial}{\partial z}\left(\rho\frac{h^3}{\eta}\frac{\partial p}{\partial z}\right)=12\frac{\partial(h\rho)}{\partial t} \tag{3}$$

Although the Reynolds equation can be used with both liquids and gases, when liquid is used other surface effects become significant and their analysis are more complicated, (Gad-el-Hak, 2006); For instance, the added mass effect, which appears because the movement of the seismic mass necessarily implies the movement of the liquid surrounding the structure. This added mass is in-phase with the plate acceleration, reducing the natural frequency and the sensitivity. In this work, it is considered that air is the fluid between the plates, and the added mass effect is of much less importace

(Marco *et. al.,* 1993). Under isothermal condition the gas density ρ is directly proportional to its pressure *p* and for perpendicular motion of the plates, the thickness *h* and density are not function of position, therefore Eq. (4) becomes, (Bech, 1983) and (Bao and Yang, 2007):

$$\frac{\partial}{\partial x}\left(p\frac{\partial p}{\partial x}\right)+\frac{\partial}{\partial z}\left(p\frac{\partial p}{\partial z}\right)=\frac{12\eta}{h^3}\frac{\partial(hp)}{\partial t} \tag{4}$$

The Eq. (5) is the Reynolds equation for isothermal squeeze-film damping of a compressible gas with negligible inertial effects, (Bao and Yang, 2007).

3.1.1. Linearized Reynolds Equation for Compressible Gas

Considering small displacement Δh of the movable plate around its balance position h_o and small pressure variation Δp around the ambient pressure p_a:

$$\begin{cases} h = h_o + \Delta h & ;\Delta h \ll h_o \\ p = p_a + \Delta p & ;\Delta p \ll p_a \end{cases}$$

Eq. (4) can be linearized as:

$$p_a\left(\frac{\partial^2 p}{\partial x^2}+\frac{\partial^2 p}{\partial z^2}\right)-\frac{12}{{h_o}^2}\frac{\partial p}{\partial t}=\frac{12\eta_o p_a}{{h_o}^3}\frac{dh}{dt} \tag{5}$$

where η_o is the viscosity coefficient of the fluid at ambient pressure. Assuming that the plate displacement has a form:

$$h = h_o + \Delta h\ \cos\omega t \tag{6}$$

and that the pressure distribuition has a parabolic profile, as shown in the Fig. 3, it is possible to obtain the solution of the Eq. (5) through Fourier series expasion, (Kampen and Wolffenbuttel, 1998).

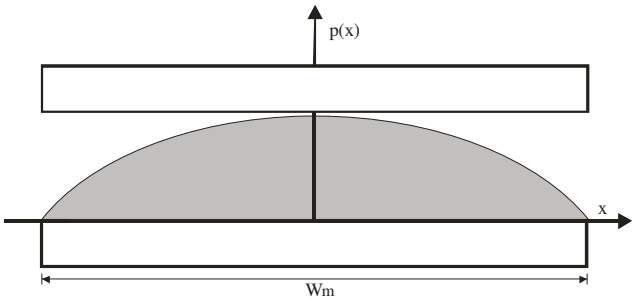

Figure 3. The pressure distribution profile between the two plates.

The solution for rectangular plates is composed of two out-of-phase components: one is related to air viscous flow, when it is squeezed out, or pulled in, the gap region. The gap pathway restricts the flow, which causes gas pressure to increase. This component is called damping force F_d and it is in-phase with the plate velocity. The other component is related to air compression and it is called elastic damping force, or only spring force, F_e. The spring force is in-phase with the plate displacement.

The damping force and spring force normalized by the displacement Δh are given by;

$$\frac{F_d(\sigma)}{\Delta h}=\frac{64\sigma}{\pi^6}\sum_{m,n\ odd}\frac{m^2+(n/\Gamma)^2}{(mn)^2\{[m^2+(n/\Gamma)^2]+\sigma^2/\pi^4\}} \tag{7}$$

$$\frac{F_e(\sigma)}{\Delta h}=\frac{64\sigma^2}{\pi^8}\sum_{m,n\ odd}\frac{1}{(mn)^2\{[m^2+(n/\Gamma)^2]+\sigma^2/\pi^4\}} \tag{8}$$

where Γ is the plate aspect ratio (ratio between the plate width W_m and the plate length L_m) and σ is the squeeze number and it is determined by:

$$\sigma = \frac{12\eta_o {W_m}^2 \omega}{p_a {h_o}^2} \tag{9}$$

The squeeze number is directly proportional to frequency what enables one to do the following analysis: in low frequency, i. e., low squeeze number, the air has enough time to escape by the borders and the viscous force dominates. On the other hand, in high frequency the air has no time to escape and it is squeezed between the two plates creating compression effects. In this case, the air behaves mainly like a "spring", and the spring force becomes dominant.

It is possible to find the transition region where the compression effects becomes equal to the viscous effects equaling Eqs. (7) and (8), so one has

$$\frac{\sigma_c}{\pi^2} = \frac{\sum_{m,n\ odd}\left(\frac{m^2 + (n/\Gamma)^2}{(mn)^2\{[m^2 + (n/\Gamma)^2] + \sigma^2/\pi^4\}}\right)}{\sum_{m,n\ odd}\left(\frac{1}{(mn)^2\{[m^2 + (n/\Gamma)^2] + \sigma^2/\pi^4\}}\right)} \tag{10}$$

where σ_c is the cut-off squeeze number, which is equal to 21.623 for a square plate ($\Gamma = 1$).

The normalized damping and spring forces in function of the squeeze number for a square plate is shown in Fig. 4.

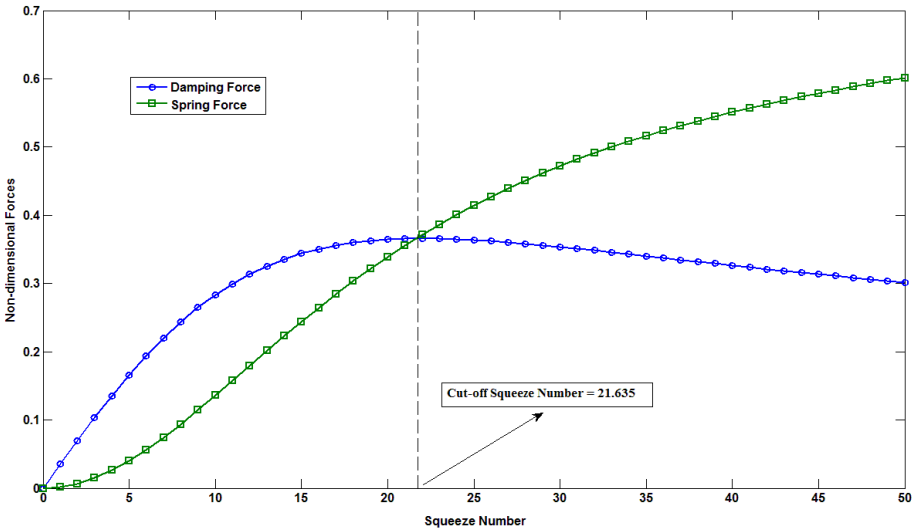

Figure 4. The normalized damping and spring forces as a function of the squeeze number for a square plate.

The solutions of Eqs. (7), (8) and (10) are obtained using a comercial mathematical software. Fig. 4 shows that for a low squeezed number ($\sigma < 0.2$), which gives ($F_d / \Delta h = 100\ F_e / \Delta h$), the compression effects can be neglected. On the other hand, when the knudsen number increases the spring force also increases and it becomes dominant after the cut-off knudsen number. With the cut-off squeeze number value is possible to establish the cut-off frequency ω_c.

The damping b_d coefficient and the spring k_e coefficient can be obtained from the Eqs. (7) and (8), respectively. For a square plate they are given by,

$$b_d(\sigma) = \frac{64\sigma p_a A}{\pi^6 h_o} \sum_{m,n\ odd} \frac{m^2 + n^2}{(mn)^2\{[m^2 + n^2] + \sigma^2/\pi^4\}} \tag{11}$$

$$k_e(\sigma) = \frac{64\sigma^2 p_a A}{\pi^8 h_o} \sum_{m,n\ odd} \frac{1}{(mn)^2\{[m^2 + n^2] + \sigma^2/\pi^4\}} \tag{12}$$

The coefficients above can be incorporated in the accelerometer dynamic model to take into account the compressibility of the air and its dependency of the movement frequency.

3.1.2. Linearized Reynolds Equation for Incompressible Gas

As discused previously, when the squeeze number is very small the compressible effects can be ignored and Eq. (4) becomes,

$$\frac{\partial^2 p}{\partial x^2}+\frac{\partial^2 p}{\partial z^2}=\frac{12\eta_o}{h^3}\frac{dh}{dt} \tag{13}$$

Eq. (13) can be solved through the series expansion with the same boundary conditions used in the compressible equation. In these conditions, the damping coefficient is given by

$$b_d=\frac{\eta_o L_m {W_m}^3 \beta(\Gamma)}{{h_o}^3} \tag{14}$$

where $\beta(\Gamma)$ is the geometrical correction factor. The geometrical correction factor for a square plate is $\beta(W_m = L_m) = 0.4217$, (Yeh and Najafi, 1997).

3.1.3 Modified Reynolds Equation

When the pressure drops below the ambient pressure the "Standard" Reynolds equation, Eq. (4) is no more applicable and the modified Reynolds Equation has to be used, (Veijola, 1995);

$$\frac{\partial}{\partial x}\left(\frac{ph^3}{\eta_o}Q_{pr}\frac{\partial p}{\partial x}\right)+\frac{\partial}{\partial z}\left(\frac{ph^3}{\eta_o}Q_{pr}\frac{\partial p}{\partial z}\right)=12\frac{\partial(hp)}{\partial t} \tag{15}$$

where Q_{pr} is the relative flow rate coefficient. This coefficient is determined using Boltzmann's transport equation and it can not be expressed in a closed form. Veijola *et. al.* (1995) derived the following approximation that differs by less than 5% from the original equation. More recently, the approximation was modified replacing K_n by $\sigma_p K_n$ to include slip-flow effects, (Veijola *et. al.*, 1998):

$$Q_{pr}=1+9.638(\sigma_p K_n)^{1.159} \tag{16}$$

where K_n is the knudsen number and σ_p is given by

$$\sigma_p=\frac{2-\alpha_v}{\alpha_v}[1.016-0.1211(1-\alpha_v)] \tag{17}$$

where α_v is the tangential momentum accommodation coefficient (TMAC) and it is defined as the fraction of molecules which are diffusively reflected. Experimental results show that silicon has TMAC of about 0.7 with several gases, (Bao and Yang, 2007) and (Gad-el-Hak, 2006).

The knudsen number is given by,

$$K_n=\frac{\lambda}{h_o} \tag{18}$$

where λ is the mean free path of gas. With this modification the Reynolds equation can be solved with the same boundary conditions used in the sections 3.1.1 and 3.1.2, therefore the damping coefficient as a funcition of the pressure for a incompressible gas is given by,

$$b_d=\frac{\eta_o L_m {W_m}^3 \beta(\Gamma)}{Q_{pr}{h_o}^3} \tag{19}$$

The same approach used in Eq. (20) can also be used in Eqs. (6) and (7) to include rarefied and slip-flow effects in a compressible gas. In some works, including Veijiola *et. al.* (1995), the ratio η_o / Q_{pr} is called effective viscosity, however, this concept is valid only up to molecular flow regime, (Gad-el-Hak, 2006).

3.1.4 Large Displament Models

The accelerometer described has a differencial configuration, thus there is another thin film of gas between the movebale plate and the upper fixed plate (upper stationary electrode). The equivalent damping coefficient can be obtained by association of dampers what is similar to spring association. In this configuration the total damping is obtained mutiplying the Eq.(14) or Eq.(19) by two, i. e, serie association.

The models described are derived under the assumption of very small displacement of the plate. Sadd and Stiffler (1975) analyzed the large displacement effects on the squeeze film damping for incompressible gas, for different geometric forms. The solution for rectangular plates is,

$$b_d = \frac{\eta_o L_m {W_m}^3 \beta(\Gamma)}{{h_o}^3}\left[1-\left(\frac{z}{h_o}\right)^2\right]^{-\frac{3}{2}} \tag{20}$$

where z is the displacement in z-direction.

Peeters *et. al*. (1991) used a simpler model derived replacing the gap by the gap minus the displacement z, for modeling the damping coefficient of a differential accelerometer.

$$b_d = \frac{\eta_o L_m {W_m}^3 \beta(\Gamma)}{{h_o}^3}\left[\frac{1}{(1-z/h_o)^3}+\frac{1}{(1+z/h_o)^3}\right] \tag{21}$$

Figure 5 shows a comparison between the linear and non-linaer models using the data from Table 1. The graph in Fig. 5 shows that for a displacement of about 20% of the gap size, the models' results are practically the same. However, for larger displacement the model used by Peeters starts to disagree with the others models. The model proposed by Sadd is more conservative and starts to disagree from linear model only for a displacement equal to 60% of gap size. The Peeter's model has been more used for damping modeling in large displacement conditions, Peeters *et. al*. (1991), Marco *et. al.* (1993), Veijola *et. al*. (1995) and the linear model was used in small displacement conditions, Andrews *et. al*. (1993), Yeh and Najafi (1997) and Kampem and Wolffenbuttel (1998). The large displacement models also can be extend by using the relative flow rate coefficient (Kaajakari, 2009). An equivalent-circuit model was used in Veijola *et. al.* (1999) to study the large displacement behavior of an capacitive accelerometer by introducing the displacement dependence in the relative flow rate coefficient.

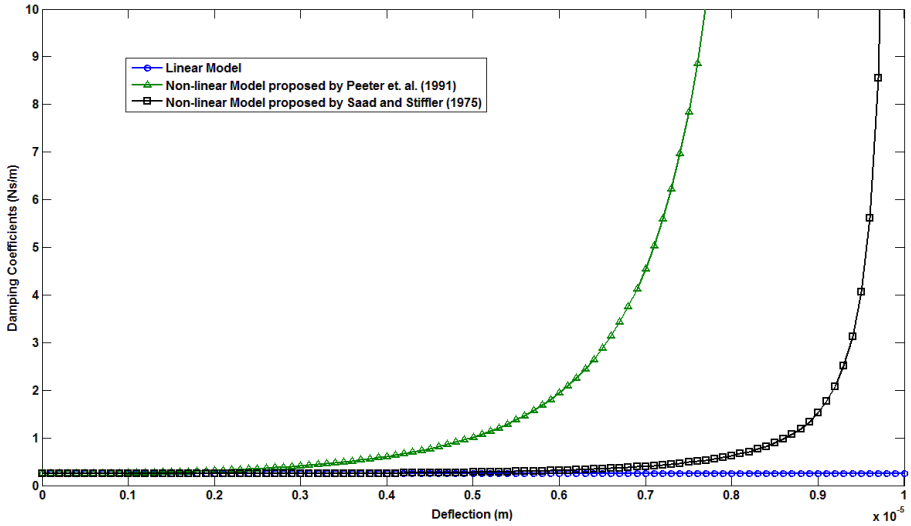

Figure 5. Comparison between the liner and non-linear models of damping coefficients.

4. RESULTS AND DISCUSSION

The Reynolds' equation in its most general form was presented. The first assumptiom done was that the inertia effects are negligible when compared with the viscous effects. This assumption can be verified through the modified Reynolds number R_S and R_L. Analizing only vertical motion of the moving plate, i. e., R_L is equal to zero. R_S can be

obtained with the data in Table 1 and the Eq. 2, what leads to $R_S = 0.0166$. Therefore, the inertia effects can be ignored. When the gap is very large or at high frequencies the model described breaks down and another model has to be used. A model including the inertia effects is presented in Veijola (2004).

Another important assumption is the isothermal condition. This can be justified due to small volumes and the big surface areas in the structure, the thermal contact between the gas and the surrounding accelerometer solid structure is very good. In addition, the silicon is a very good thermal conductor. For these reasons, it is safe to assume that the gas is isothermal, (Gad-el-Hak, 2006).

The Linearized Reynolds equation is obtained under assumptions of small displacement around the gap thickness and small pressure deviation around the ambient pressure. When the displacement becomes larger the non-linear model has to be used. The gas rarefied effects and slip-flow effects can be used to model damping in pressure smaller than the ambient pressure. When both conditions are not satisfied a special approach including a large displacement model with relative flow rate coefficient can be used.

The Linearized Reynolds equation solution takes into account the gas compression effects. The importance of these effects can be analyzed by the squeeze number. The squeeze number for this accelerometer model is 0.219, which means that the damping force is approximately two orders of magnitude bigger than the spring force. Therefore, the gas compression effects can be ignored; hence, incompressible solution can be utilized. Both values calculated for the Reynolds number and the squeeze number were over-estimated due to the fact that the accelerometer has to work far bellow of its resonance frequency.

The analytical results were obtained using a transfer function of a classical second order mechanical system with the natural frequency and the effective mass, both in Table 1. Eq. (19) was used to calculate the viscous damping coefficient with different pressure values. Considering silicon as the plates material and air as the gas between them, when the pressure p is equal to the ambient pressure p_a, the relative flow rate coefficient is equal to 1.060 and Eq. (19) tends to Eq. (14). A previous mechanical analysis has shown that for an acceleration of 1g the linear model described in this equation is enough, (Rodrigues *et. al.*, 2011).

The simulated results were obtained using the 3D model and the commercial software COMSOL Multiphysics®. This software has the modified Reynolds equation as part of its CFD package, COMSOL (2010). The simulations were done using PC with an Intel® Core™ i7 processor, 4GB Dual Channel DDR3 SDRAM memory and 500GB (5400RPM) Hard-Drive. The solution time was about 7 hours for each value of pressure, using a tetrahedral mesh with 38,701 elements.

The Fig. 6 shows a comparison between the analytical and the CFD results for step input of 1g.

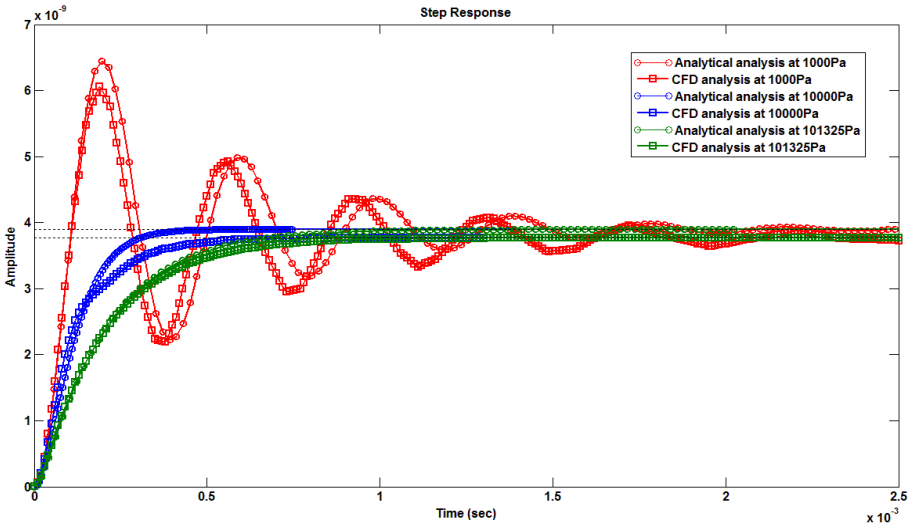

Figure 6. Analytical and CFD time response for step input of 1g.

The simulations were done for tree different pressure values. The pressure values are 10^3Pa, 10^4Pa and the ambient pressure which leads a knudsen numbers of 0.006823, 0.06913, 0.69 and the relative flow rate coefficients of 1.060, 1.872 and 13.570, respectively. Fig. 6 shows the system changing from an under-damper system into an over-damped system.

Figure 6 also shows that the analytical results in the time-domain are in aggrement with the CFD results and it represents perfectly the three characteristics of the system: under-damping, critically-damped and over-damped. There is a little difference of 4% in the amplitude between the analytical and the CFD results, however the settling times are approximately the same.

The following figures show the comparison between the results in the frequency-domain for different pressure values. The amplitude response as a function of the frequency is shown in Fig. 7 and the phase response is shown in Fig. 8. These figures show that the analytical results in the frequency -domain are in very good agreement with the CFD ones. The small difference observed at amplitude in the time domain response is not observed anymore in the frequency domain, due to the fact that it takes into account the normalized amplitude.

It is well known that for a classical oscillator with linear damping, a maximum bandwidth is attained when a damping ratio of 0.7 is set. Therefore, with the damping coefficient is possible to calculate the exactly pressure that leads this damping ratio. Comparison between the analytical model and the experimental results are given in Andrews *et. al.* (1993), Veijola *et. al.* (1995) and Bourgeois *et. al.* (1997). However, it is important to highlight that when one works with pressure bellow the ambient pressure in micro-scale, some of the vacuum issues, as for example gas leaks, become a big problem.

As can be seen in Eq. (20) the damping coefficient is highly dependent on the gap size, i.e., the bandwidth optimization also can be done by controlling the gap size. However, in capacitive accelerometers the gap size has a fundamental importance from the electrical point of view, so it has not a free range. Another way to control damping is through perforations in the plate; however it increases the micromachining process complexity.

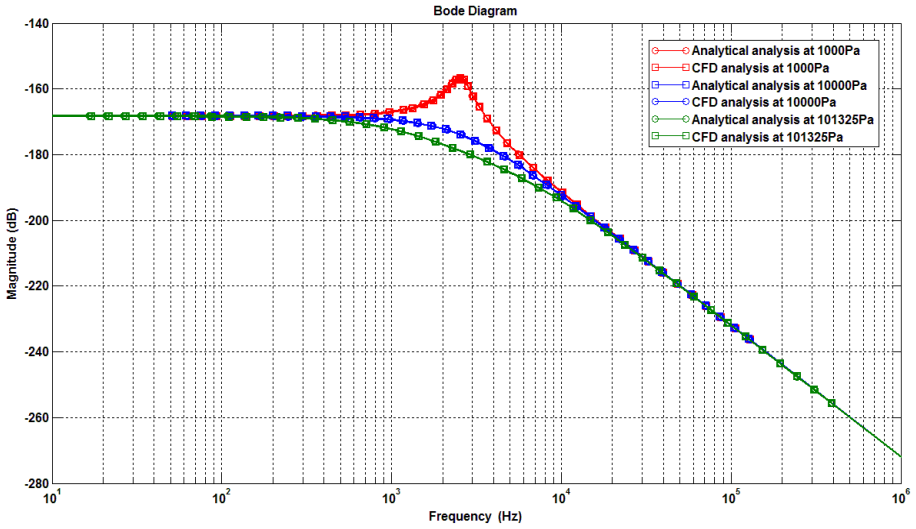

Figure 7. Analytical and CFD results to magnitude versus frequency.

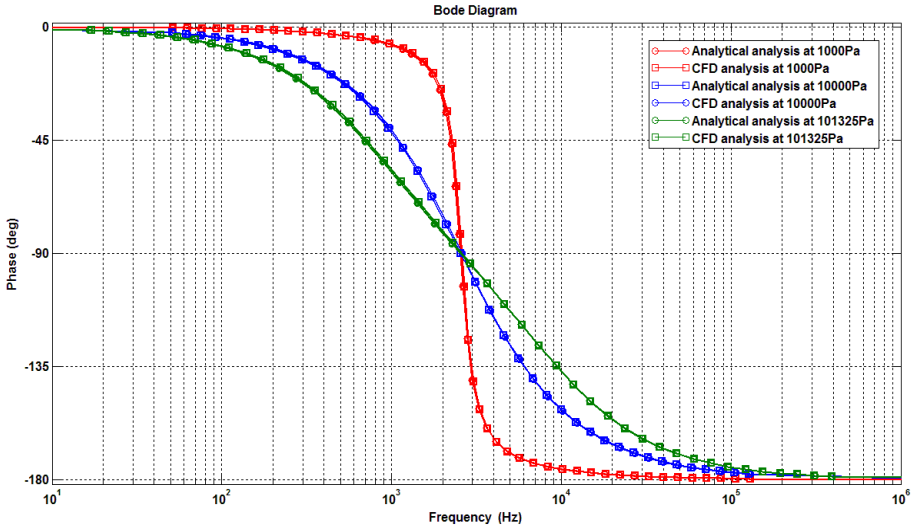

Figure 8. Analytical and CFD results of phase versus frequency.

5. CONCLUSION

The accurate detemination of the main damping mechanism is of great technological importance to characterization and optimization of the inertial microdevices.

The results obtained in this work by applying the analytical model presented for damping analysis of a differential capacitive accelerometer are quite accurate when compared with the CFD results. Moreover, as expected, solving the problem by applying the analytical model is much faster than obtaining the CFD solutions.

The next step is to run the 3D accelerometer model with the transient solution of the full Navier Stokes Equation, which costs much more in terms of computational resources. However, it will give a much better idea of the analytical solution accuracy.

6. ACKNOWLEDGEMENTS

This work was supported by FINEP (Brazilian Agency for Funding of Studies and Projects), under grant n: 01.09.0395.00, project ACELERAD. The authors also thanks the financial support of CNPQ (National Council for Research and Development) under grants: 310768/2009-8, 311082/2009-2, and 303689/2009-9.

7. REFERENCES

Andrews, M., Harris, I. and Turner, G., 1993, "A Comparison of Squeeze-Film Theory With Measurements on a Microstructure",Sensor and Actuators A, Vol. 36, pp. 79–87.

Bao, M. and Yang, H., 2007, "Squeeze film air damping in MEMS", Sensor and Actuators A, Vol. 136, pp. 3–27.

Blech, J. J, 1983, "On Isothermal Squeeze Films", Transaction of the ASME Journal of Lubrication Technology, Vol. 105, pp. 615–620.

Bode, H, A., 2002, "Análise do Movimento de Eixos Sustentados por Mancais do Tipo Squeeze Film", In Portuguese, Master degree dissertation presented at Aeronautics Institute of Technology, Brazil, São José dos Campos, 138 pp.

Bourgeois, C., Porret, F, and Hoogerwerf, A., 1997, "Analytical Modeling of Squeeze-Film Damping in Accelerometers", Intern. Conference on Solid-State Sensors and Actuators, Chicago, Illinois, USA, June 16-19.

COMSOL Multiphysics, 2010, "Squeeze-Film Gas Damping in an Accelerometer", COMSOL user's manual.

Gad-el-Hak, M., 2006, "The MEMS Handbook", Ed. CRC Taylor & Francis, New York, USA, 200 p.

Kaajakari, V., 2009, "Practical MEMS", Ed. Small Gear Publishing, Louisiana, USA, 496 p.

Kampen, R. P. V. and Wolffenbuttel, R. F., 1998, "Modeling the Mechanical Behavior of Bulk-Micromachined Silicon Accelerometer", Sensor and Actuators A, Vol. 64, pp. 137–150.

Marco, S., Samiter, J., Ruiz, O., Herms, A. and Morante, J. R., 1993, "Analysis of Electrostatic-Damped Piezoresistive Silicon Accelerometer", Sensor and Actuators A, Vol. 37-38, pp. 317–322.

Peeters, E., Vergote, S., Puers, B. and Sansen, W., 1991, "A Highly Symmetrical Capacitive Micro-Accelerometer With Single Degree-of-Freedom Response", Proceedings of the 6th International Conference Solid-State Sensors and Actuators (Transducers' 91), San Francisco, CA, USA, June 24-28, pp 97-100.

Rodrigues, J. R., Teves, A. C., Passaro, A., Góes, L. C. S., Silva, E. C. N and Mateus, C. F. R., 2011, "Static Mechanical Analysis of a Bulk-Micromachined Accelerometer", Proceedings of the 21st Brazilian Congress of Mechanical Engineering, Natal, Rio Grande do Norte, Brazil, October 24-28.

Sadd, M. and Stiffler, A, K., 1975, "Squeeze Film Damping: Amplitude Effects at Low Squeeze Numbers", Transaction of the ASME Journal of Engineering for Industry, pp. 1366–1370.

Veijola, T., Kuisma, H., Lahdenpara, J. and Ryhanen, T., 1995, "Equivalent-Circuit Model of Squeezed Gas in a Silicon Accelerometer", Sensor and Actuators A, Vol. 48, pp. 239–248.

Veijola, T., Kuisma, and Lahdenpara, J., 1998, "The Influence of Gas-Surface Interaction on Gas-Film Damping in a Silicon Accelerometer", Sensor and Actuators A, Vol. 66, pp. 83–92.

Veijola, T., Kuisma, H. and Lahdenpara, J., 1999, "Compact Large-Displacement Model for a Capacitive Accelerometer", Proceedings of the 2nd International Conference on Modeling and Simulation of Microsystems, Semiconductors, Sensors and Actuators., Puerto Rico, USA, April 19-21, pp. 218–221.

Veijola, T., 2004, "Compact models for squeezed-film dampers with inertial and rarefied gas effects", Journal of Micromechanics and Microengineering, Vol. 14, pp. 1109–1118.

Yeh, C. and Najifi, K., 1997, "A Low-Voltage Tunneling-Based Silicon Microaccelerometer", IEEE Transaction on Electron Devices, Vol. 44, Nº11, pp. 1875–1882

8. RESPONSIBILITY NOTICE

The authors are the only responsible for the printed material included in this paper.